Fusion Engineering and Design 161 (2020) 111869

Contents lists available at ScienceDirect

Fusion Engineering and Design

journal homepage: www.elsevier.com/locate/fusengdes

Eddy current analyses for vacuum vessel of CFQS quasi-axisymmetric stellarator

Takanori Murase[a,*], Sho Nakagawa[a], Shigeyoshi Kinoshita[a], Akihiro Shimizu[a,b], Shoichi Okamura[a], Mitsutaka Isobe[a,b], Guozhen Xiong[c], Yuhong Xu[c], Haifeng Liu[c], Hai Liu[c], Dapeng Yin[d], CFQS team[a,c,d]

[a] National Institute for Fusion Science, 322-6 Oroshi, Toki, Gifu 509-5292, Japan
[b] The Graduate University for Advanced Studies, SOKENDAI, 322-6 Oroshi, Toki, Gifu 509-5292, Japan
[c] Institute of Fusion Science, School of Physical Science and Technology, Southwest Jiaotong University, Chengdu 610031, People's Republic of China
[d] Hefei Keye Electro Physical Equipment Manufacturing Co., Ltd, Hefei 230000, People's Republic of China

ARTICLE INFO

Keywords:
Eddy current
Finite element method
Quasi-axisymmetric
CFQS

ABSTRACT

The design activity on the CFQS quasi-axisymmetric stellarator which is conducted as a joint international project is ongoing by National Institute for Fusion Science (NIFS) in Japan and Southwest Jiaotong University (SWJTU) in China. The CFQS magnetic field generating coils consist of sixteen modular coils (MCs) in total with four different types, four poloidal field coils (PFCs), and twelve toroidal field coils (TFCs). In designing fusion devices, eddy currents and electromagnetic (EM) forces on the vacuum vessel (VV) have to be evaluated to verify the mechanical confidence and reliability. In this work, we consider the following three issues, (1) Influence of eddy current induced by external coil current change on the CFQS magnetic confinement, (2) Evaluation of EM force on VV by eddy current under a typical current of the MC and the PFC, and (3) Feasibility check of whether it is possible to heat the CFQS VV by using induction current.

1. Introduction

The construction of the world's newest quasi-axisymmetric stellarator CFQS is ongoing as a joint project of National Institute for Fusion Science (NIFS) in Japan and Southwest Jiaotong University (SWJTU) in China [1–3]. The CFQS has the advantages of both tokamak system with good plasma confinement performance [4] and helical system with excellent sustainability for plasma discharge [5]. The physics design of the CFQS has been completed, and the engineering design such as the magnetic field generating coil and the vacuum vessel (VV) has been eagerly advanced [6].

In the design of a fusion device, it is crucial to verify the influence of eddy currents for the mechanical confidence and reliability. In the tokamak device, electromagnetic (EM) analysis has been performed to predict the eddy current induced by disruption, which is a plasma collapse phenomenon [7–9]. On the other hand, regarding the helical device using a superconducting coil, eddy currents induced on VV by quenching, which is a loss of the superconducting state, due to the phase transition of liquid helium pose a problem [10]. In a helical device using normal conducting coils, since the energization time of magnetic field coils is generally limited by the balance between heat generation and cooling performance of coils, the plasma discharge duration is also limited. Due to this restriction, the influence of the eddy current generated by changing the coil current may be exerted during the plasma discharge.

In the plasma experiment, the EM force generated in the VV results in repeated stress at every plasma discharge. If the stress exceeds the design stress and the elastic-region even locally, there is a possibility that a fatigue fracture of stainless steel will occur, which greatly affects the reliability and durability of the VV. Therefore, we must investigate the reliability of the CFQS VV in advance.

Gases such as nitrogen, oxygen, hydrogen, water vapor, and carbon dioxide are adsorbed on the inner wall of a VV under the atmospheric pressure, and these adsorbed gases are released as outgas from a VV inner wall during the vacuum pumping. Since these outgases hinder the high vacuum pumping process, it is necessary to heat up the entire VV by heaters such as tape-shaped heaters around the outer wall of the VV in general, and to release the adsorbed gas attached to the inner wall. As for a baking method for the CFQS VV, usage of an induction heating with an eddy current generated in the VV has been proposed [6]. We

* Corresponding author.
E-mail address: murase.takanori@nifs.ac.jp (T. Murase).

https://doi.org/10.1016/j.fusengdes.2020.111869
Received 10 March 2020; Received in revised form 4 July 2020; Accepted 7 July 2020

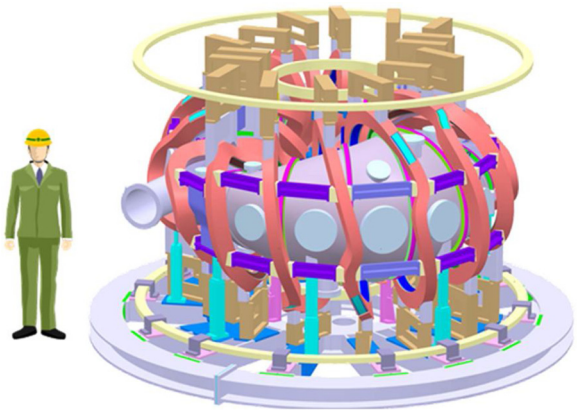

Fig. 1. Bird's eye view of CFQS.

must check the feasibility of adopting the induction heating in the CFQS from the engineering point of view.

In this paper, the finite element analysis (FEA) codes, ANSYS Maxwell for EM analysis, and ANSYS Mechanical for structural analysis, were employed in order to verify the EM issues described above for the CFQS.

2. Coil system and vacuum vessel design for CFQS

The physical properties of the CFQS are as follows: toroidal periodic number $N = 2$, aspect ratio $A_p = 4$, magnetic field strength $B_t = 1$ T, major radius $R_0 = 1$ m, and typical rotational transform *iota-bar* in vacuum ranges from 0.35 to 0.4 in the entire region of plasma. Fig. 1 shows a bird's-eye view of CFQS, and Fig. 2 shows the external view of the CFQS VV (Fig. 2(a)) and the CFQS coil system (Fig. 2(b)). The CFQS

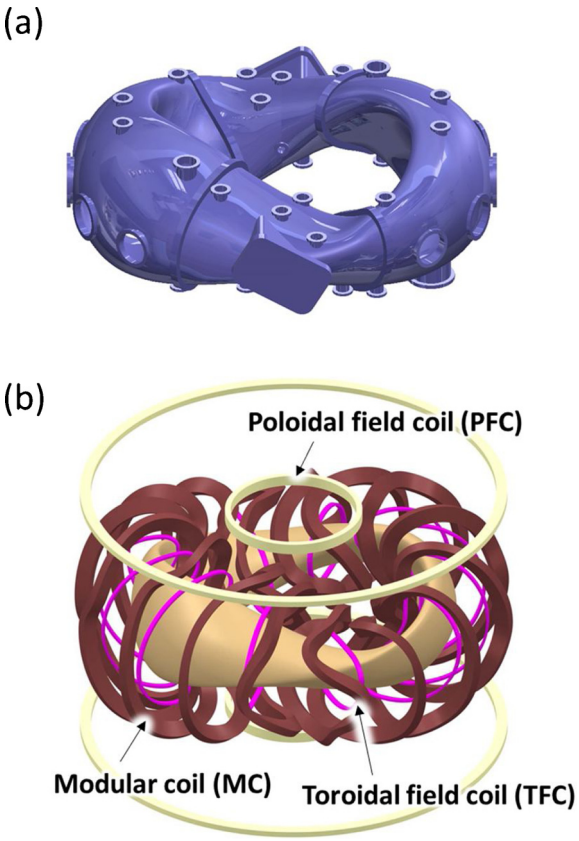

Fig. 2. External view of (a) vacuum vessel and (b) magnetic field generating coil system.

VV is made of stainless steel and has over 40 ports for plasma heating and diagnostics. The CFQS coil system consists of 4 difference-shapes of 16 modular coils (MCs), 4 poloidal field coils (PFCs), and 12 toroidal field coils (TFCs) for generating a magnetic field to confine plasma.

The CFQS VV is made of relatively thin stainless steel (SUS316 L, thickness of 6 mm), and has a complicated three-dimensional (3-D) surface. Therefore, in order to predict the EM force acting on the CFQS VV in advance, it is necessary to perform computational analyses in consideration of a 3-D structure by using FEA.

The MCs are connected in a series and supplied with an alternating current (AC) for the CFQS baking. The main motivation for using the induction heating are that (1) the cost of winding tape-shaped heaters is expected to be high due to poor workability because the between the VV and the MC is as small as about 20 mm, (2) since only one small power supply is required in the induction heating method, a low-cost baking system can be realized. Therefore, it is worth considering the induction heating method from the viewpoint of cost reduction. In order to heat the VV to the desired temperature, it is indispensable to check the feasibility of induction heating by confirming the specifications of the baking power supply, such as the current and the voltage generated on the MC.

3. Time constant of eddy current

3.1. Evaluation eddy current based on time constant

An eddy current is induced in the VV by a change in the current of the external coils. Actually, eddy currents have innumerable eigenmodes. However, in this study, we investigated the main mode of time constants, that is, the mode that seems to have the longest time constant. This relationship can be approximately expressed using the following equivalent circuit equation.

$$L\frac{dI_{VV}}{dt} + RI_{VV} = V = M\frac{dI_{PFC}}{dt} \tag{1}$$

Where I_{VV} is a total eddy current induced in the VV, I_{PFC} is a total current flowing in the PFC, L and R are the inductance and resistance of the VV, respectively, and M is the mutual inductance between the PFC and the VV. Here, if the right hand side of Eq. (1) is a constant value, that is, when the PFC current increases / decreases at a constant rate, Eq. (1) can be analytically solved, and the eddy current is given by the following equation.

$$I_{VV} = I_0\left(1 - e^{-\frac{t}{\tau}}\right) \tag{2}$$

Where, I_0 is the maximum value of the eddy current, and τ is the time constant of the eddy current determined by L/R. Note that the time constant τ does not depend on the current value of the PFC, and can be a useful method for evaluating the time to reach flattop or the remaining time of the eddy current. As shown in Fig. 3, when $t = \tau$, the value of the eddy current is about 63 % of the maximum value, when $t = 3\tau$, the value of the eddy current is about 95 % of the maximum value, and when $t = 5\tau$, the eddy current is about 99 % of the maximum value. Therefore, if the plasma discharge is performed at a time of 5τ or more after the rise of the PFC current, we can consider that the influence of the eddy current is almost eliminated. Therefore, the purpose of this section is to obtain the time constant of the eddy current.

3.2. Numerical model and conditions

Fig. 4 shows the FEA model. In this analysis, the eddy current induced in the CFQS VV by PFC was calculated. The PFC current was set to increase linearly from the time of 2 ms–40 ms, and then was set to be constant as shown in Fig. 5. A magnitude or a rate of change of the PFC current does not affect τ, hence, the magnitude of the PFC current does not affect for investigation concerning τ of the eddy current. Fig. 6

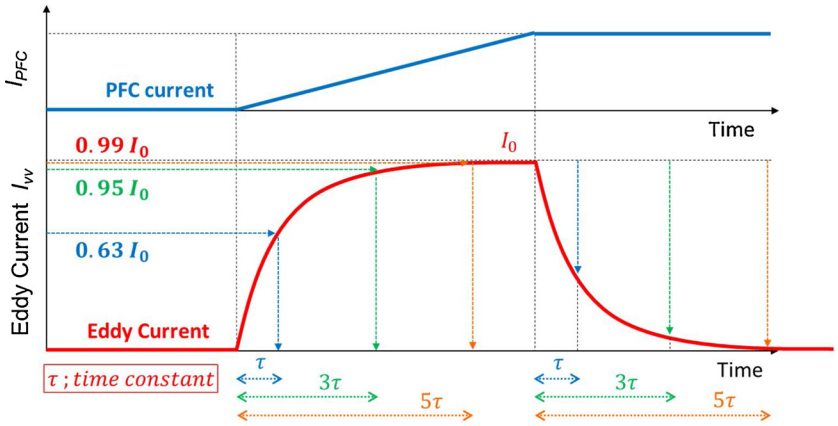

Fig. 3. Relationship between a time evolution of eddy current due to PFC and the time constant.

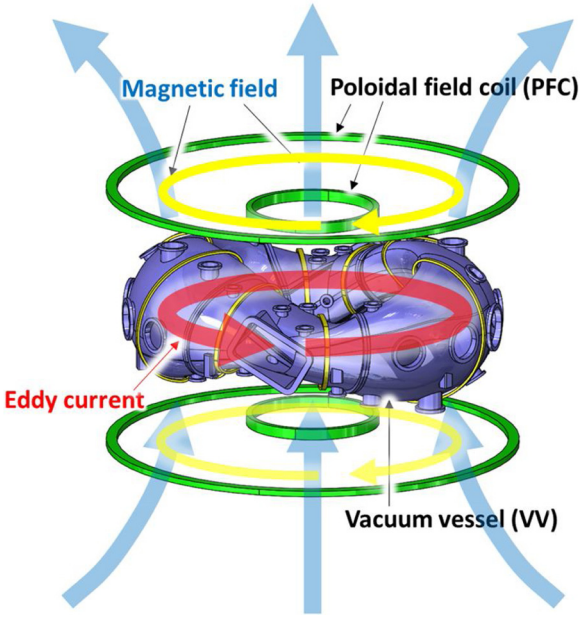

Fig. 4. FEA model for eddy current analysis. Eddy current is induced by PFC current change.

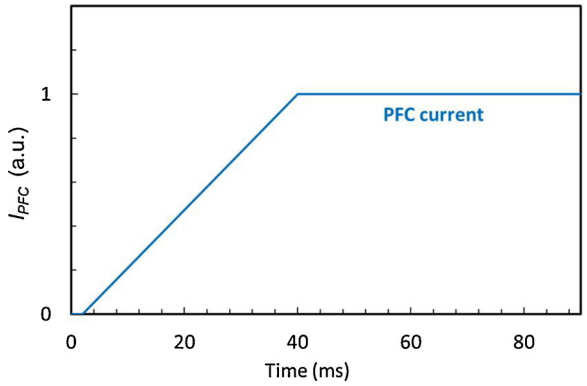

Fig. 5. Input data of PFC current to calculate time constant of eddy current.

shows the calculation meshes used in this FEA. In order to detect the eddy current induced in the VV accurately, fine calculation meshes were arranged in the VV model. The average element size in the entire analytical model is 36.14 mm (minimum element size is 0.03 mm). The number of VV elements is 267,454, and the entire analytical model is 501,532. In this eddy current analysis, transient analysis is required to calculate the eddy current induced by the time variation of the PFC. In order to accurately evaluate the change in the eddy current, it is necessary to make the time step fine. The time step Δt was set to 0.2 ms in this analysis. A rectangular computational domain was designed to enclose the CFQS VV, the PFC. Also, the Neumann boundary condition, which is a natural boundary condition, is applied to the boundary surface of the analysis region. Set the magnetic field H so that it satisfies $(\nabla \times H) \times n = 0$ on the boundary surface. Where, n is the normal vector to the boundary surface.

3.3. Results and discussions

Fig. 7 shows a result of the eddy current density distribution at the time of 40 ms. the eddy current flows counterclockwise as seen from the top, and a relatively high current density appears near diagnostics ports. This result is consistent with the theoretically expected trend. To calculate the total eddy current induced in the CFQS VV, it is necessary to integrate the current density in a cross section perpendicular to the direction in which the eddy current flows. Fig. 8(a) shows an integral cross section for calculating the total eddy current. Fig. 9 shows the time evolution of the standardized total eddy current. From the current waveform in Fig. 9, the time constant τ is approximately 4 ms. In addition, by using the integral cross-section in the Fig. 8(b), the eddy current caused by the MCs and the TFCs were analyzed in the same manner, and the time constant τ was approximately 2 ms for the MCs and the TFCs, respectively. Fig. 10(a) shows a typical current scenario of the MC current and the PFC current in the CFQS plasma experiment. The plasma discharge begins to start 50 ms after the PFC current reaches the flat top. Considering the waveform of the eddy current in an increasing period of the PFC current, there is a relationship between the eddy current and the plasma discharge time as shown in Fig. 10(b). The remaining time of the eddy current ($5\tau \sim 20$ ms) is shorter than the duration between the time at the PFC current reaching the flat top and the start of the plasma discharge (50 ms). Hence, the impact on the plasma discharge is expected to be negligibly small. Further, the resistance R and the inductance L of the VV are obtained by using the time constant of eddy current and magnetic energy obtained from the result of the FEA. In order to obtain a resistance of the VV in the toroidal direction, the developed FE model and simple electric analysis are also used. Here, the magnetic energy U_M is given by the following equation.

$$U_M = \frac{1}{2} L I_{vv}^2 = \frac{1}{2} \int_0^V B \bullet H \, dV \tag{3}$$

Where, the integral region "V" means the entire analysis region, so B and H are integrated over the analysis region in ANSYS Maxwell. Since I_{VV}, U_M, and τ are known, the resistance R and the inductance L of the VV can be calculated by the following equations.

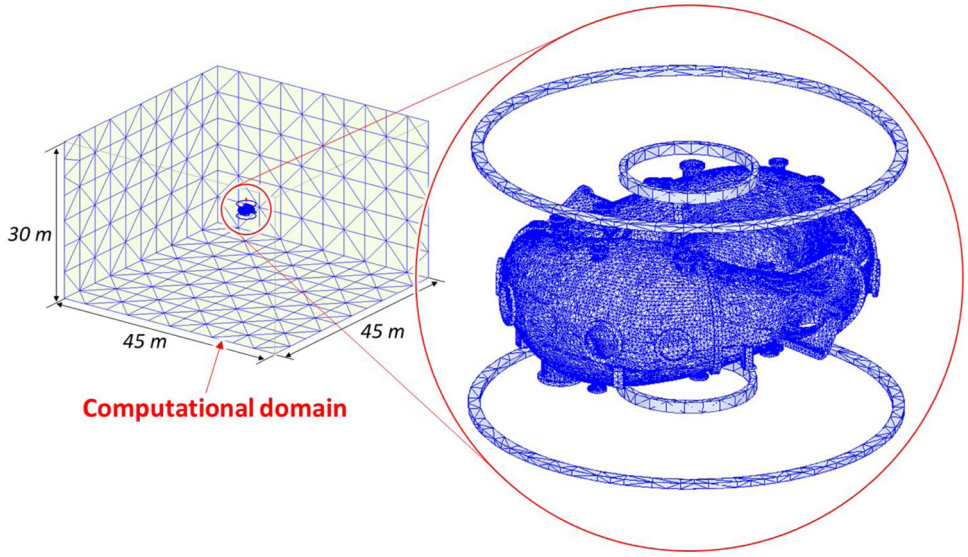

Fig. 6. Computational meshes of vacuum vessel and PFC in CFQS and computational domain to calculate the magnetic field induced by PFC current.

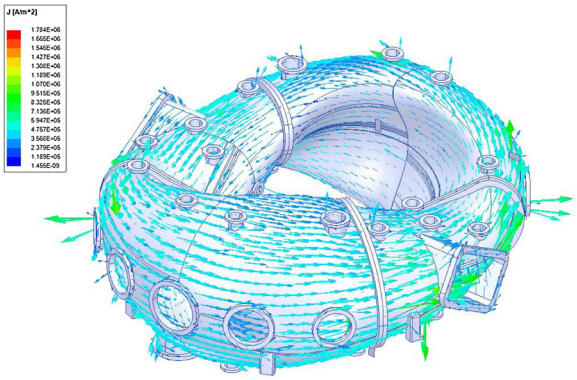

Fig. 7. Distribution of eddy current induced by PFC changing linearly (at 40 ms).

$$L = \frac{2U_M}{{I_{vv}}^2} \; and \; R = \frac{L}{\tau} \tag{4}$$

Therefore, the one-turn resistance and inductance of the CFQS VV in the toroidal direction can be estimated to be approximately 0.4 mΩ and 1.8μH, respectively. And also, in the case of MC and TFC, that is, the inductance and resistance in the poloidal direction are 0.14 μH and 0.058 mΩ, respectively. In a medium-sized tokamak, a Joule heating is required during experiment. In general, a one-turn voltage of the VV is applied to be about 10 V for a Joule heating. If the one-turn resistance of the VV is 0.4 mΩ, a large current as much as several tens of kA flows through the VV. In this case, a one-turn break is required in order to increase the one-turn resistance of the VV. However, since we do not conduct Joule heating in the CFQS VV, there is no need to consider the one-turn break or bellows. This result will contribute to the reduction of VV construction costs.

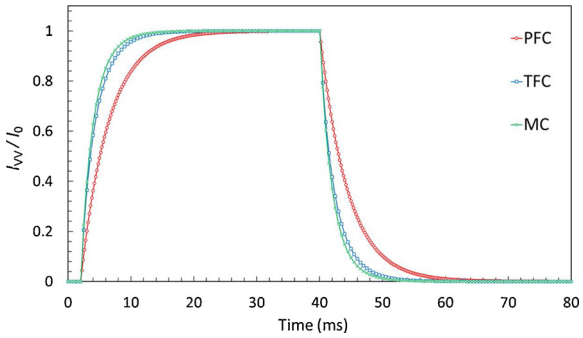

Fig. 9. Time evolution of standardized total eddy current on vacuum vessel induced by PFC, TFC, and MC.

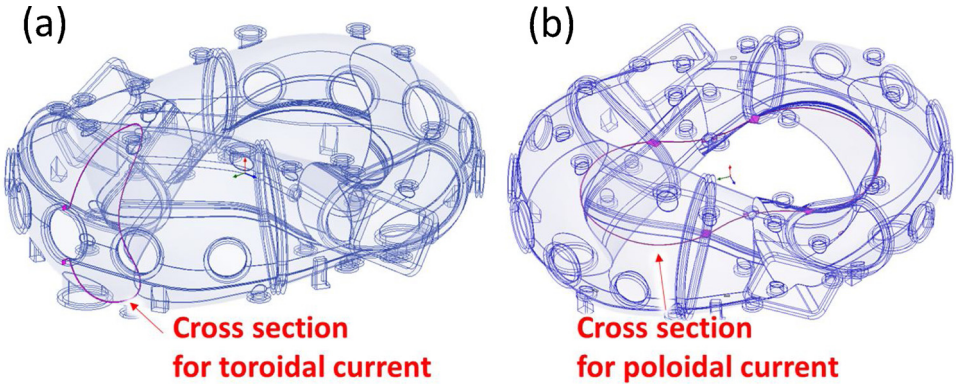

Fig. 8. Cross section to calculate total eddy current induced (a) by PFC and (b) by TFC and MC.

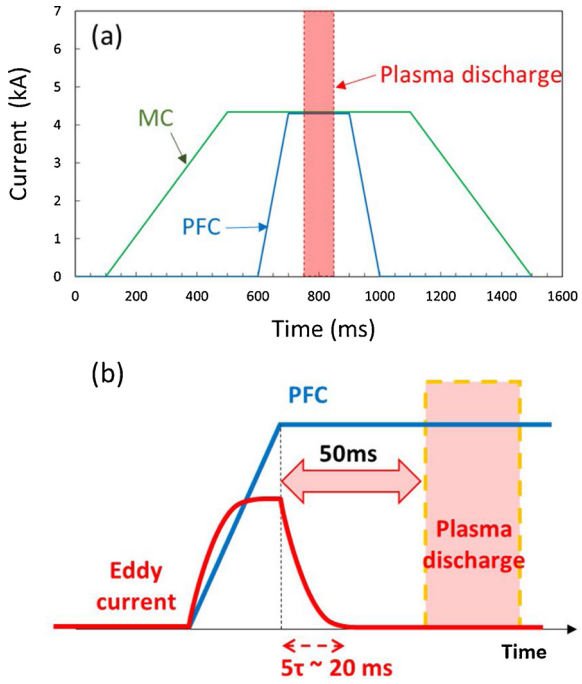

Fig. 10. (a) Typical current scenario of MC current and PFC current in CFQS plasma experiment. (b) relationship between eddy current and plasma discharge.

4. Electromagnetic force on CFQS vacuum vessel

4.1. Numerical model and conditions

EM force is generated on the CFQS VV by the interaction between the magnetic field and the eddy current due to the MC current. As shown in Fig. 10(a), the typical current scenarios of the PFC and the MC were used in this analysis. The current change rates of the MC and the PFC are 10.75 kA / s and 43 kA / s, respectively. The maximum current of the MC is 4.3 kA and the number of turns is 72. Regarding the PFC, the maximum current is 4.3 kA and the number of turns is 32. The EM force and the EM stress under this current scenario were investigated by using ANSYS Maxwell and ANSYS Mechanical. The MC is the winding coil and each MC conductor has a hollow structure [6]. However, the analysis model of the MC was designed as one bulk conductor to reduce computational costs such as a CPU time and a required memory. In the case of considering the MC as a single bulk body, the current density in the cross section of a MC is biased due to a time variation of current and becomes higher on the coil surface. In this ANSYS analysis, similar to the actual 72 winding coils, we assumed the uniform current density in a MC cross section. In this EM analysis, transient analysis is also required to calculate the EM force induced by the time variation of the MC and the PFC. The time step Δt was also set to 1 ms in this analysis.

4.2. Results and discussion

Fig. 11(a) shows the time evolution of the maximum EM force per volume (N/m^3), in the VV under the typical current scenario mentioned above. The maximum EM force increases almost linearly with the rise of the MC current. This indicates that the eddy current induced by the MC is relatively small and its influence time is short. Thereafter, the EM force is generated again with the rise of the PFC current. However, we found that the EM force is smaller than the EM force caused by the MC current. Moreover, we also found that the direction of the EM force during the falling of the MC currents (t = 1,100 ms) is opposite to that at startup (t =500 ms) as shown in Fig. 11(b) and (c). In the case of PFCs, since the EM force is generated by the outer product of the eddy current induced by the PFC current and the magnetic field induced by the MC current, the direction is opposite between the rising and falling of the PFC current. Here, if the maximum EM force in this analysis is converted into the EM pressure on the VV, the maximum EM pressure is about 0.4 atm in consideration of the thickness of the stainless steel plate of 6 mm. Although the maximum EM pressure is lower than the atmospheric pressure (1 atm), it is not a negligible value. Therefore, a structural analysis was performed by using ANSYS Mechanical with the maximum EM force obtained in the above analysis. Fig. 12 shows the boundary conditions in this analysis. Not only EM force but also vacuum force due to atmospheric pressure should be taken into account. In this study, it is assumed that VV is always exhausted during the experiment. However, there is a possibility that the current of the coil is erroneously driven when the VV is not evacuated. Fig. 13 shows the distribution of stress generated in the VV under the boundary condition mentioned above. The maximum stress of about 97 MPa occurs near the upper diagnostic port. It is less than 117 MPa, which is the allowable stress of stainless steel at room temperature [11]. Therefore, the CFQS VV has enough strength to withstand the vacuum force and the EM force generated during the experiment. Note that there is no appropriate standard to apply to VV of fusion experimental devices, we adopt ASME Section III, which is the standard for nuclear vessel, as a design standard that is often used. In the case of only evacuation, the maximum von Mises stress acting on the CFQS VV is approximately 87.4 MPa, the effect of only eddy current is approximately 10 MPa. Furthermore, since the maximum stress is within an elastic deformation range, there is also no possibility that the CFQS VV will break due to repeated stress fluctuations. To confirm the mechanical confidence of the CFQS VV, it is necessary to consider also safety margin for VV buckling under pressure and EM loads and effect of baking and welding. They will be investigated in future study.

5. Induction heating for CFQS vacuum vessel baking

5.1. Numerical model and conditions

For the CFQS VV baking method, an induction heating method has been considered as a baking method for VV, in which 16 MCs are connected in a series and an AC is applied to the MC to generate heat by resistance loss of eddy current generated in the VV. In this analysis, the AC analysis is required to calculate the heat generation of the CFQS VV by the induction current induced by the MCs. In general, when an AC flows through a conductor, a skin effect appears in which the current density is high at the surface of the conductor and gradually decreases with distance from the surface. If the skin depth δ is smaller than the thickness of the VV (6 mm), it can be considered that the eddy current concentrates on the VV surface. In this case, since a layered thin and fine mesh is required on the surface of the VV even in the FEA, the skin depth must be considered in advance. Here, skin depth δ can be calculated by the following equation.

$$\delta = \sqrt{\frac{2}{2\pi f \mu_r \mu_0 \sigma}} \quad (5)$$

Note that this skin depth formula is obtained for semi-infinite materials, and for toroidal vacuum vessels the skin depth may be shorter. Where f is the AC frequency, μ_r is the relative magnetic permeability, μ_0 is the vacuum magnetic permeability, and σ is the electric conductivity of the VV. When the skin depth is calculated using Eq. 5, for example in the case of f = 2 kHz, the skin depth δ is approximately 9 mm. Therefore, since the skin depth is larger than the plate thickness of the VV, we considered that the current concentration due to the skin effect does not occur on the CFQS VV surface.

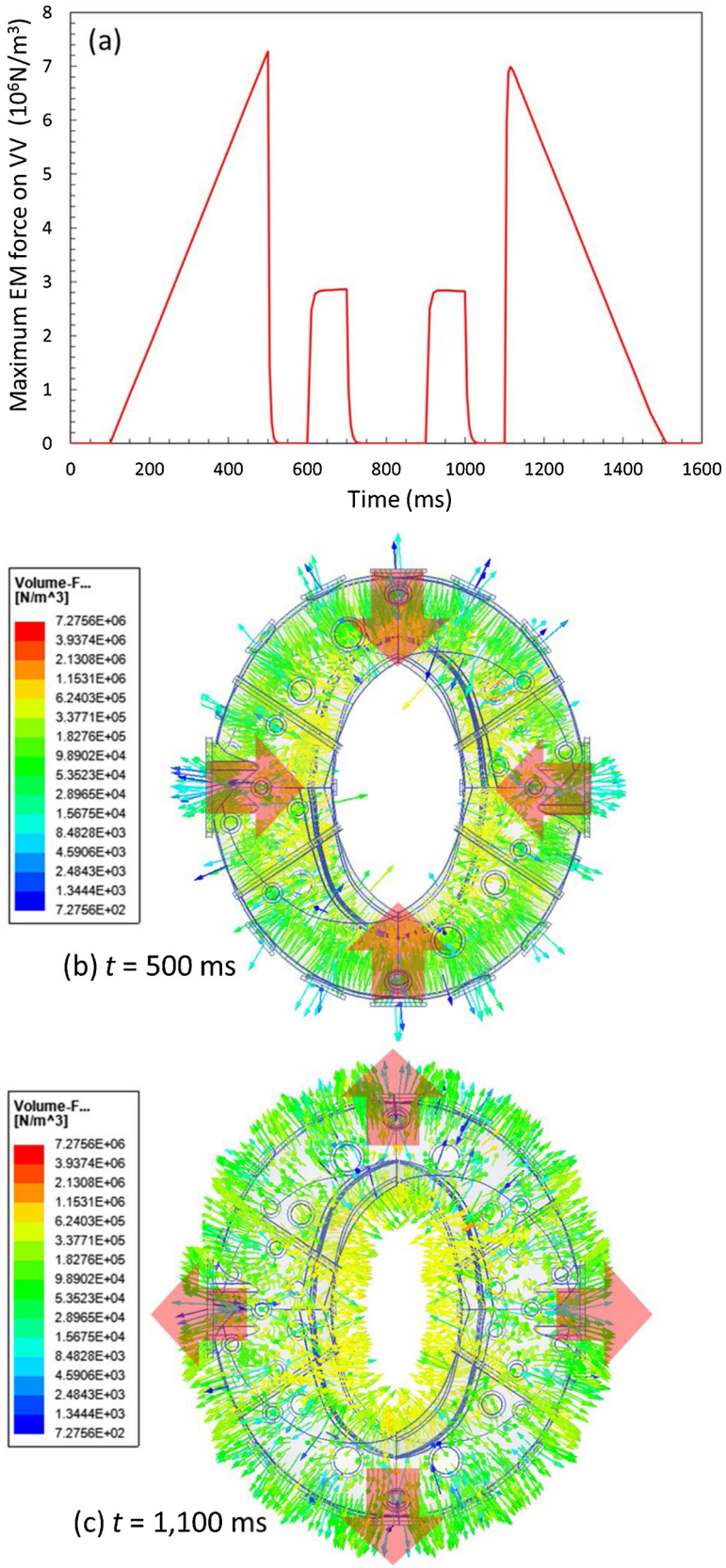

Fig. 11. (a) Maximum EM force on CFQS VV under typical current scenario, and Distribution of EM force (b) at 500 ms, (c) at 1,100 ms.

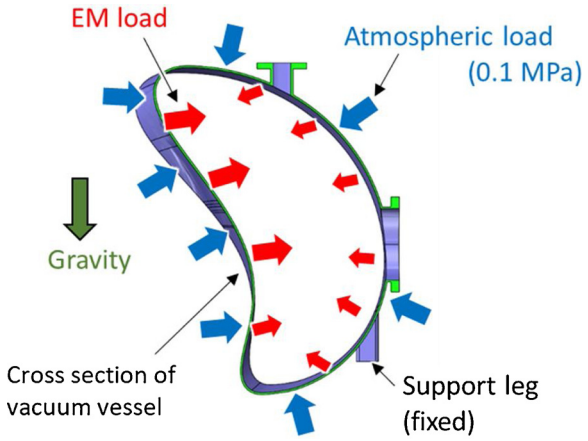

Fig. 12. Boundary conditions for structural analysis under the condition considering maximum EM load and atmospheric load.

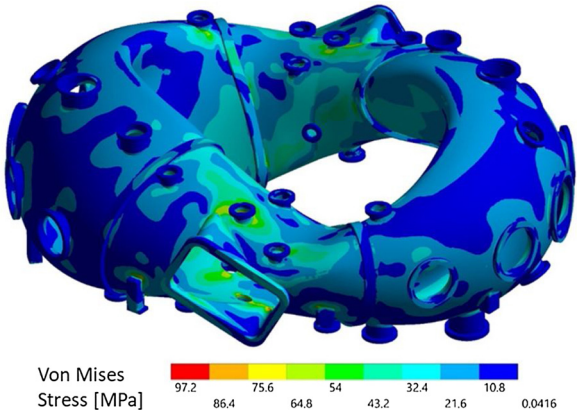

Fig. 13. Distribution of von Mises stress in the CFQS VV under condition taking maximum EM load and atmospheric load into account. Maximum stress is approximately 97.2 MPa.

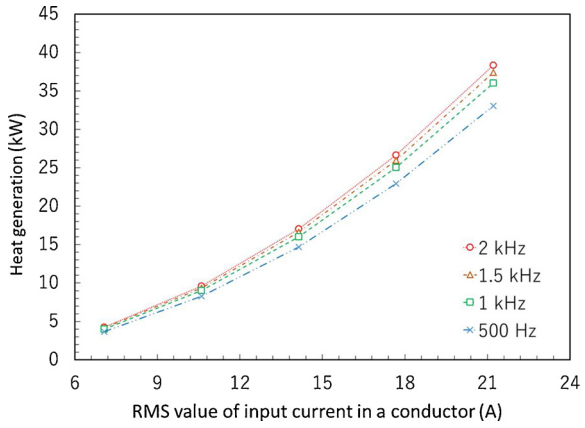

Fig. 14. Heat generation with changing RMS value of input current in a conductor and AC frequency. Number of MC and turns are 16 and 72, respectively.

5.2. Results and discussion

The heat generation of the CFQS VV with the current value and AC frequency of MC changing was investigated by using ANSYS Maxwell as shown in Fig. 14. The Root Mean Square (RMS) value I_{AC} of input current in a conductor was changed from about 7 A to 21 A, and the AC frequency was investigated at 500 Hz, 1 kHz, 1.5 kHz, and 2 kHz. Fig. 15 shows an example of the heat distribution of the VV obtained by this analysis in the case of $f = 1$ kHz and $I_{AC} = 7$ A. It can be seen that the heat generation is more strongly dependent on the current value than the AC frequency. Here, the heat generation required for baking in the CFQS VV is 25 kW. This value is determined based on the actual value of VV baking system of Compact Helical System (CHS) [12] which has a similar size to the CFQS. In this case, the current required for the CFQS VV baking can be obtained to be about 18 A from Fig. 14. The voltage applied in the MC is obtained by this current value I_{AC} and AC resistance ωL as follows.

$$V_{MC} = I_{AC} \cdot \omega L \tag{6}$$

Where ω is the angular frequency represented as $2\pi f$. The self-inductance and mutual inductance for 16 MCs were calculated by using ANSYS Maxwell. The inductance L in Eq. (6) is about 0.3 H obtained by the sum of each inductance. Substituting $I_{AC} = 18A$, and $f = 1kHz$ into Eq. 6, the applied voltage on the MC is obtained to be approximately 34 kV. As a result, this voltage value exceeds the operation voltage of DC 2.4 kV. Therefore, we found that the induction heating method could not be adopted in the CFQS. An alternative method should be considered as a next option, for example, the sheathed heater system. As an alternative candidate, even in case of small gap, PTC baking method may be adopted as in SUNIST of Tsinghua University.

6. Summary

Using the finite element analysis code, ANSYS Maxwell, the eddy current generated in the VV of the CFQS quasi-axisymmetric stellarator was investigated. From the time constant of the eddy current, it was found that the influence of the eddy current on the plasma discharge was negligible. In addition, the EM force generated in the VV was calculated in the typical current scenario of the MC and the PFC. Since the maximum EM force is about 0.4 atm, which is not negligible compared to the atmospheric pressure, structural analysis was performed by using ANSYS Mechanical. In this analysis, the EM force during plasma experiments and vacuum force due to atmospheric pressure were considered. As a result, we found that the maximum stress value was less than the allowable level of stainless steel and the CFQS VV has sufficient strength. In addition, the induction heating, which has been considered as a baking method of the CFQS, was verified, and we found that the adoption of the induction heating method is difficult because the applied voltage in the MC exceeded the allowable voltage. The above findings will contribute to engineering design and operation for the CFQS.

CRediT authorship contribution statement

Takanori Murase: Formal analysis, Software, Investigation, Writing - original draft. **Sho Nakagawa:** Software, Investigation. **Shigeyoshi Kinoshita:** Resources, Methodology, Writing - review & editing. **Akihiro Shimizu:** Project administration, Writing - review & editing, Supervision. **Shoichi Okamura:** Supervision. **Mitsutaka Isobe:** Supervision, Writing - review & editing. **Guozhen Xiong:** Software, Investigation. **Yuhong Xu:** Project administration. **Haifeng Liu:** Supervision. **Hai Liu:** Supervision. **Dapeng Yin:** Supervision.

Declaration of Competing Interest

The authors declare that they have no known competing financial interests or personal relationships that could have appeared to influence the work reported in this paper.

Acknowledgments

The authors are thankful for strong support and encouragement of this project (NSJP) from Director General Prof. Y. Takeiri of NIFS and

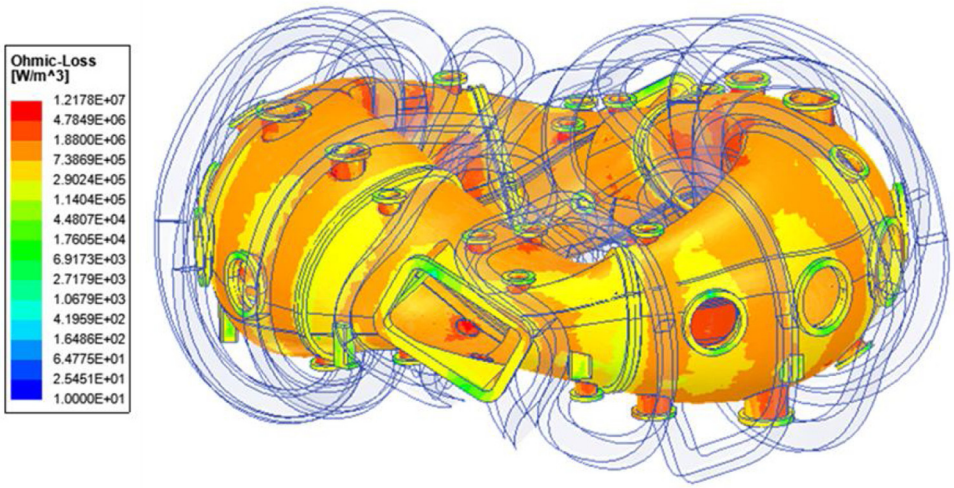

Fig. 15. Distribution of the heat generation in case of I_{AC} = 7 A, f = 1 kHz. The maximum heat generation in VV is approximately 1.2e7 W/m^3.

former Vice President Prof. W.G. Zhang of SWJTU. The authors are also grateful for the support to the NSJP from other related staff of NIFS and SWJTU. This research is supported by NIFS general collaboration project, budget number NIFS18KBAP041, NIFS17KBAP034, NIFS17KLPP048, NIFS budgetURSX401, UFEX105, and Post-Core University Program (CUP) for Japan-China collaboration in magnetic confined fusion. This research is supported also by the National Science Foundation of China under Grant No. 11820101004.

References

[1] H. Liu, et al., Plasma Fusion Res. 13 (2018) 3405067.
[2] A. Shimizu, et al., Plasma Fusion Res. 13 (2018) 3403123.
[3] M. Isobe, et al., Plasma Fusion Res. 14 (2019) 3402074.
[4] ITER Organization, ITER Research Plan Within the Staged Approach (level III—provisional Version) ITER Technical Report ITR-18-003, (2018).
[5] Y. Takeiri, et al., Nucl. Fusion 57 (2017) 102023.
[6] S. Kinoshita, et al., Plasma Fusion Res. 14 (2019) 3405097.
[7] H. Jhang, et al., Fusion. Eng. Des. 65 (2003) 629–641.
[8] S. Sakurai, et al., Fusion. Eng. Des. 84 (2009) 1684–1688.
[9] Y. Zhai, et al., Fusion. Eng. Des. 88 (2013) 547.
[10] K. Koizumi, et al., J. Plasma Fusion Res. 72 (1996) 1352–1361.
[11] ASME Boiler and Pressure Vessel Code, Section III, Rules for Construction of Nuclear Facility Components, (2010).
[12] K. Matsuoka, et al., Plasma physics and con-trolled nucl. fusion res, IAEA, Vienna, 1988 Proc. 12thInt. Conf. Nice, 1988, Vol. 2 1989, p. 411.